PCCP

ROYAL SOCIETY OF CHEMISTRY

PAPER

View Article Online
View Journal | View Issue

Cite this: *Phys. Chem. Chem. Phys.*, 2024, **26**, 17334

Modelling the growth reaction pathways of zincone ALD/MLD hybrid thin films: a DFT study†

Mario Mäkinen, *[a] Timo Weckman [b] and Kari Laasonen [a]

Received 18th January 2024,
Accepted 23rd May 2024

DOI: 10.1039/d4cp00249k

rsc.li/pccp

ALD/MLD hybrid thin films can be fabricated by combining atomic layer deposition (ALD) and molecular layer deposition (MLD). Even though this deposition method has been extensively used experimentally, the computational work required to acquire the reaction paths during the thin film deposition process is still in dire demand. We investigated hybrid thin films consisting of diethyl zinc and either 4-aminophenol or hydroquinone using both gas-phase and surface reactions to gain extensive knowledge of the complex phenomena occurring during the process of hybrid thin film deposition. We used density functional theory (DFT) to obtain the activation energies of these kinetic-dependent deposition processes. Different processes of ethyl ligand removal as ethane were discovered, and we found that the hydroxyl group of 4-aminophenol was more reactive than the amino group in the migration of hydrogen to an ethyl ligand within a complicated branching reaction chain.

1 Introduction

Atomic layer deposition (ALD) is a method to fabricate thin films with thicknesses in the nanometer range. In addition to the exceptional thinness of the fabricated thin films, this method can also be used to fabricate homogeneous thin films on uneven surfaces. During ALD, gaseous precursors are released into the reactor individually and sequentially. Each precursor can only react with surface molecules, and, therefore, the precursor is attached to the surface as a layer with a theoretical thickness of one atom. Excess residue of this precursor is then removed from the reactor using some inert gas, usually nitrogen.[2]

Based on ALD, another method, called molecular layer deposition (MLD), has also been developed, in which polymer chains are made from organic precursors. ALD has been developed since the 1970s and MLD has been developed since the 1990s. The atomic/molecular layer deposition (ALD/MLD) makes it possible to combine these methods and thus use both inorganic and organic layers of the atoms together as hybrid thin film materials.[3] Future applications of these hybrid thin films include electrode and coating materials for battery applications, solar cells, UV-active photoluminescence materials, flexible, lightweight magnets, catalytic applications, and protective coatings.[4] The fabrication process of hybrid thin films is still rather unknown from the perspective of chemical reaction mechanisms due to the very difficult experimental access to the properties of the transition state structure. The chemical reactions used to fabricate these hybrid materials are adsorption reactions, which can be studied using density functional theory (DFT) modelling. Thus, we can reveal the chemistry occurring in the reactor during the thin film fabrication process. This enables the fine-tuning of the deposition process and the feasibility comparison between precursors, which can enable the discovery of completely new precursors and deposition processes.

Zinc is one of the most common elements in conventional ALD due to the high demand for ultrathin zinc oxide structures in microelectronic applications.[4,5] Similar to ALD, in the ALD/MLD processes, diethyl zinc is the most common inorganic precursor, and it is often combined with an organic precursor hydroquinone.[4–12] To prevent hydroquinone from reacting twice within the same precursor pulse, Sood *et al.*[13] suggested the use of 4-aminophenol, which replaces one of the two hydroxyl groups of hydroquinone with an amino group, to promote more sequential growth of the thin film due to the different reactivities of the reacting functional groups.

The hybrid thin films under investigation consisted of diethyl zinc and an organic phenol, either 4-aminophenol or hydroquinone, depending on the thin film. These zincone thin films have been studied using both gas-phase models and

[a] *Department of Chemistry and Materials Science, School of Chemical Engineering, Aalto University, Kemistintie 1, 02150, Espoo, Finland. E-mail: kari.laasonen@aalto.fi*
[b] *Department of Chemistry, University of Jyväskylä, Survontie 9 B, 40500, Jyväskylä, Finland*

† Electronic supplementary information (ESI) available: The *xyz* coordinates of the reactions studied are included in the supplementary material. With these coordinates the systems can be visualized, and with an appropriate DFT code our results can be reproduced. This data, along with the relevant metadata and the results of the Bader charge analysis, are also presented in the Harvard Dataverse.[1] See DOI: https://doi.org/10.1039/d4cp00249k

significantly more computationally expensive surface models. The surface models consisted of two different ethyl-saturated zinc oxide surfaces and the adsorbing organic precursor of the first precursor pulse. The organic precursor is adsorbed onto the zinc oxide surface *via* a branching chain reaction pathway, leading to either a ligand exchange or a dissociation reaction. 4-Aminophenol reacts faster with its hydroxyl group than with its amino group. The key step in the total hybrid thin film growth reaction was discovered to be the removal of the ethyl group as ethane. Different ethyl removal processes were discovered and found to depend on the coverage of the ethyl ligands on the zinc oxide surface.

1.1 Experimental results by other groups

Hybrid thin films made of diethyl zinc with either hydroquinone[6–12] or 4-aminophenol[13,14] have been extensively researched experimentally. Hydroquinone and diethyl zinc were used by Yoon *et al.*[8] to fabricate hybrid thin films. With a deposition temperature of 150 °C, uniform and electron-conducting thin films were fabricated. The growth rate was 1.6 Å per cycle, and the total number of cycles was 1000. Yoon *et al.*[9] also combined hydroquinone and diethyl zinc layers with layers made of water and diethyl zinc to fabricate conductive and transparent thin films. The electron conductivity of the thin films was controlled by varying their composition. Even though pure zincone thin films have much lower electron conductivity than zinc oxide thin films, the thin films containing both structures combined can have a higher conductivity than pure zinc oxide thin films. Liu *et al.*[10] discovered that thermal conductivity can also be varied by varying the content of water, diethyl zinc, and hydroquinone in these films. This effect of varying the thermal conductivity was also discovered by Tynell *et al.*,[11] who discovered that the thermal conductivity of zinc oxide can be lowered by implementing one layer of hydroquinone every 50th or 100th deposition cycle. Karttunen *et al.*[12] deposited these hybrid thin films on cotton textile substrates.

Sood *et al.*[13] investigated the use of heterobifunctional 4-aminophenol in zincone hybrid thin films. Two different functional groups and the stiff backbone of the aromatic ring should prevent double reactions of the precursor within the same precursor pulse. These double reactions are undesirable because they hinder the growth of the thin films, as the precursor cannot react further with the diethyl zinc of the next precursor pulse. Zincone hybrid thin films were deposited on top of 40 zinc oxide layers. The deposition temperature ranged from 140 to 330 °C. The growth of the thin film was linear, with an approximate growth rate of 1.1 Å. The hybrid films were stable in the ambient atmosphere, even at relatively high humidity levels, when capped with few zinc oxide layers. The films were reported to be amorphous, and the FTIR spectra revealed that both the hydroxyl and amino groups were bonded to zinc. Hybrid thin films fabricated with varying ratios of 4-aminophenol, diethyl zinc, and water were investigated by Sundberg *et al.*[14] The ratio between the components was found to alter the hardness, chemical stability, surface roughness, density, and crystallinity of thin films. 4-Aminophenol can be removed from the structure using acetone, but this can be prevented by a 10 nm-thick topmost layer of zinc oxide.

1.2 Computational work by other groups

Computational work related to the zincone hybrid thin films under study is relatively scarce. Zincone thin films were studied by Karttunen *et al.*,[15] who studied superlattice structures, where a small layer of hydroquinone was surrounded by a ZnO crystal structure. They discovered that a chemical bond between every zinc atom of the zinc oxide surface and hydroquinone would lead to noticeable repulsive interactions between the adsorbed hydroquinone molecules, which can be lowered by halving the amount of hydroquinone on the surface. They also discovered that the band structure of the superlattice could be tailored by varying the organic content of the thin film. In addition, Choudbury *et al.*[16] studied zincone hybrid thin films using diethyl zinc (in the form of hydroxylated monoethyl zinc) and hydroquinone as precursors in a gas-phase model. They found that layers of zinc oxide stabilized the structure of the zincone hybrid thin film *via* a more exothermic reaction between the bonded monoethyl zinc and water than bonded monoethyl zinc and hydroquinone. They also discovered the hydroxylated monoethyl zinc molecule to have a reaction energy of −0.9 eV at room temperature when bonding with hydroquinone.

Quite recently, computational research studies have been conducted on titanicone[17] and alucone[18,19] hybrid thin films. Tanskanen *et al.*[17] studied the thermodynamics of the reactions of both hydroquinone and 4-aminophenol with $TiCl_4$, which were adsorbed onto a TiO_2 surface. They found that both the hydroxyl and amino groups of 4-aminophenol can bind to Ti^{4+}-ions and that the hydroxyl group binds more strongly than the amino group. Muriqi *et al.*[18] studied the thermodynamics of reactions between the methyl-terminated Al_2O_3 surface and both hydroquinone and 4-aminophenol. Both amino and hydroxyl groups bind favorably with either Al–O or Al–N bonds and eliminate CH_4 from the surface. The hydroxyl group was found to be more reactive than the amino group. Yang *et al.*[19] studied the gas-phase reaction between trimethyl aluminum and both 4-aminophenol and hydroquinone. They discovered that aluminum binds tightly to the hydroxyl group while eliminating H and CH_3. This reaction is irreversible until all methyl groups are consumed. The reaction between the amino group and trimethyl aluminum is reversible. The reaction sequence was found to be considerably slower for the amino group than for the hydroxyl group.

1.3 Growth reactions of the ALD/MLD hybrid thin films

The precursors responsible for the growth of the hybrid thin films investigated in this study are presented in Fig. 1. The surface reactions studied in this work are both the ligand-exchange reaction presented in Fig. 2 and the dissociation reaction presented in Fig. 3. Later, the hydrogen donated in the dissociation reaction can migrate to an ethyl ligand, thus cleaving ethane from the surface. The migration reaction is presented in Fig. 4.

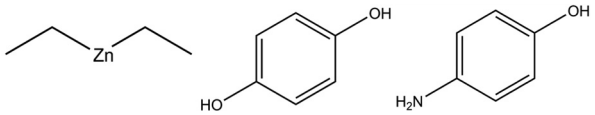

Fig. 1 Precursors used to build ALD/MLD hybrid thin films investigated in this study: diethyl zinc (left) reacted either with hydroquinone (middle) or 4-aminophenol (right).

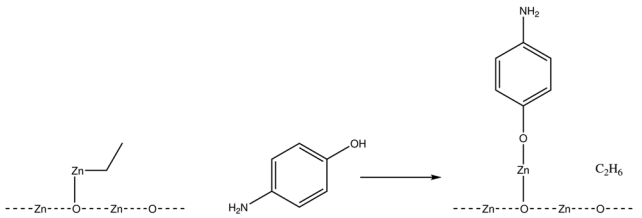

Fig. 2 Ligand-exchange reaction investigated in this study, which grows ALD/MLD hybrid thin films: diethyl zinc reacted previously with the surface to create monoethyl zinc, which now reacts with 4-aminophenol resulting in the removal of gaseous ethane.

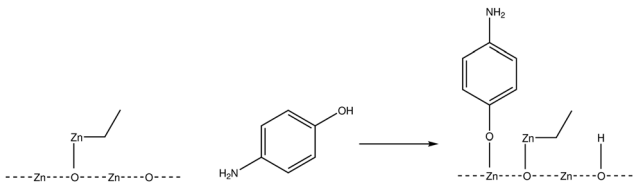

Fig. 3 Dissociation reaction investigated in this study, which grows ALD/MLD hybrid thin films: 4-aminophenol donates hydrogen to the surface structure, thus adsorbing to the surface without reacting with monoethyl zinc.

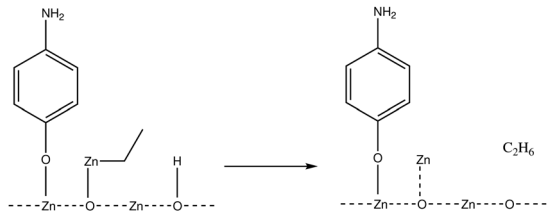

Fig. 4 Migration reaction investigated in this study, which grows ALD/MLD hybrid thin films: after dissociation reaction presented in Fig. 3, the hydrogen originally from 4-aminophenol can migrate to an ethyl ligand and cleave it as ethane from the surface.

The macrostructure of the thin film can be either a more traditional hybrid thin film, where a single layer of organic molecules and a metal atom alternate, or a more unconventional superlattice structure, where layers of single organic molecules are surrounded by relatively thick zinc oxide layers. The differences between the hybrid thin film and superlattice structures are presented in Fig. 5.

The reactions between the precursors presented in Fig. 1 were studied using DFT calculations. The energy ΔE of these reactions can be calculated by subtracting the energy of the initial state E_{init} from the energy of the reacted state E_{fin}, which

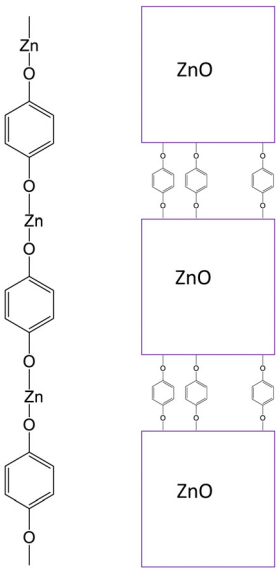

Fig. 5 The final composition of the film can be a hybrid thin film, where metal atoms and organic molecules alternate (presented on the left), or a superlattice structure, where organic molecule layers are surrounded by relatively thick zinc oxide layers (presented on the right).

corresponds to the final state of the reaction. The activation energy E_{act} for the reaction between the precursors can be calculated using the energy of the highest energy state, *i.e.* the transition state E_{ts} along the minimum energy path from the initial state to the final state of the reaction, and subtracting E_{init} from E_{ts}. One can also calculate the energy of the molecular adsorption $\Delta E_{\text{m.ads}}$. of the precursor molecule on the ethyl-saturated zinc oxide surface using eqn (1),

$$\Delta E_{\text{m.ads.}} = E_{\text{init}} - E_{\text{meox}} - E_{\text{adsorbate}} \quad (1)$$

where E_{init} is the total energy of the molecular adsorption system, which is also the initial state of the chemisorption reaction. E_{meox} is the energy of the ethyl-saturated zinc oxide slab, and $E_{\text{adsorbate}}$ is the total energy of an independent molecule 4-aminophenol.

2 Computational methods

Modelling of the reaction pathways was conducted using GPAW[20] with an atomic simulation environment (ASE).[21] Visual molecular dynamics (VMD)[22] program was used in the visualization of the results. Density functional theory (DFT) was used with the Perdew–Burke–Ernzerhof (PBE) exchange and correlation functional.[23] The DFT description is known to provide a drastic underestimation of the band gap of the ZnO bulk band structure.[24] The effect of this underestimation on the reaction energies was tested using the Hubbard+*U*-correction[25] with parameters from Calzolari *et al.*[24] The effect on the reaction energies was found to be minute, and therefore, this correction was not used in the calculations. However, van der Waals correction TS09, by Tkatchenko and Scheffler,[26] was utilized to account for the weak interactions between a large aromatic

precursor and ethyl ligands, which can have a noticeable contribution to the reaction energy of the system. The real-space grid spacing was 0.2 Å, and the sampling of the *k*-space was conducted with a 2 × 2 × 1 Monkhorst–Pack grid. The criterion for convergence was a force smaller than 0.05 eV Å^{-1} on all individual atoms, which offers a good balance between accuracy and computational efficiency. All of the reaction barriers were calculated using the nudged elastic band method with a climbing image,[27] utilizing a chain of 10 images of the system and a FIRE[28] optimizer. Bader analysis[29] was used to determine the absence of abnormal changes in the oxidation states of atoms during the reactions. These results are included in the Harvard Dataverse.[1]

Due to the large number of rotational degrees of freedom of the ethyl ligands present in the studied ethyl-saturated zinc oxide surfaces, 3 ps molecular dynamics (MD) simulations with 1 fs time steps were used to effectively probe the potential energy surface. Then, geometry optimization was used for the generated structures between 500 fs intervals to find a minimum for the given surface structure. A small polarized double-ζ basis set was used for the dynamic simulations. The temperature was kept constant at 450 K using a Berendsen thermostat to prevent unwanted decomposition, which could be caused by a temperature that is too high. Additionally, relaxed surface scans were employed to determine an energetically favorable structure for the physisorption of 4-aminophenol onto the zinc oxide surface. The reaction coordinate was chosen to be the distance between the nitrogen or oxygen atom of the functional group of 4-aminophenol and the chosen zinc atom in the surface structure. Then, using constrained optimization, the surface was probed along the reaction coordinate.

The use of DFT, especially when not paired with a relatively computationally expensive hybrid functional, can lead to an underestimation of activation energies of chemical reactions.[30] This study focuses on the relative comparison of the transition state energies and the detection of reaction paths with relatively high activation energies. Even if the real reaction barriers are slightly higher than our results, this would not change the conclusions of our work. Despite these limitations in the calculations of absolute energies, DFT is recognized as the most viable and, thus, widely used approach to gather information about the chemical reaction rates for complicated surface reactions.[31–33] DFT can also be utilized in the *ab initio* molecular dynamics,[34] which can aid in the research of dynamical systems, but this approach is useful only if reaction rates are fast, which is not the case for the chemical reactions investigated in this study.

3 Results

3.1 Gas-phase reactions

Gas-phase reactions were used to model the ligand elimination reactions that occur on the surface during the deposition of organic precursors. The studied gas-phase reactions consisted of a 4-aminophenol or hydroquinone precursor that reacted with a diethyl zinc molecule. 4-Aminophenol can either react with an amino or a hydroxide group, and therefore, reactions with both functional groups were investigated. Due to the similarities between the reactions of the hydroxide group in both 4-aminophenol and hydroquinone molecules, the surface reactions of both hydroquinone and 4-aminophenol were studied using only a 4-aminophenol molecule. Along with the data regarding hydroquinone, the activation energies of both reactions containing 4-aminophenol (presented in Fig. 6 and 7) are listed in Table 1.

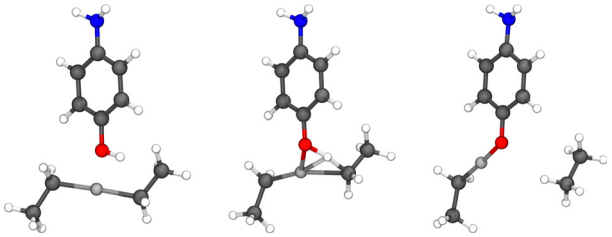

Fig. 6 Initial state (left), transition state (middle), and final state (right) of the reaction between the hydroxyl group of 4-aminophenol and diethyl zinc. This reaction is very similar to that between hydroquinone and diethyl zinc. The colors of the atoms in the figure: oxygen in red, nitrogen in blue, hydrogen in white, zinc in light grey, and carbon in black.

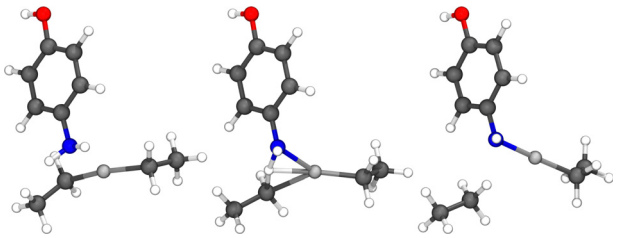

Fig. 7 Initial state (left), transition state (middle), and final state (right) of the reaction between the amino group of 4-aminophenol and diethyl zinc molecule. The atom colors are the same as those in Fig. 6.

Table 1 Reaction parameters of the studied gas-phase reactions: diethyl zinc reacts with either 4-aminophenol or hydroquinone

Precursor reacting with diethyl zinc	E_a (eV)	ΔE (eV)
Hydroquinone	0.9	−0.7
4-Aminophenol (hydroxyl group)	0.8	−0.7
4-Aminophenol (amino group)	1.5	−0.1

3.2 Surface reactions

Two ethyl-ligand-saturated zinc oxide surface slabs were used in this study. These surfaces model the experimental system presented in the experimental work by Sood *et al.*,[13] where the base layer of hybrid thin films consists of 40 ALD cycles of alternating diethyl zinc and water pulses, thus forming zinc oxide. The final diethyl zinc pulse leaves the surface saturated with monoethyl zinc, and thus the first organic precursor pulse of the ALD/MLD-thin film reacts with monoethyl zinc.

As the forming thin film of an ALD process is dependent on numerous variables such as temperature, the actual structure of the model benefits when it is benchmarked against

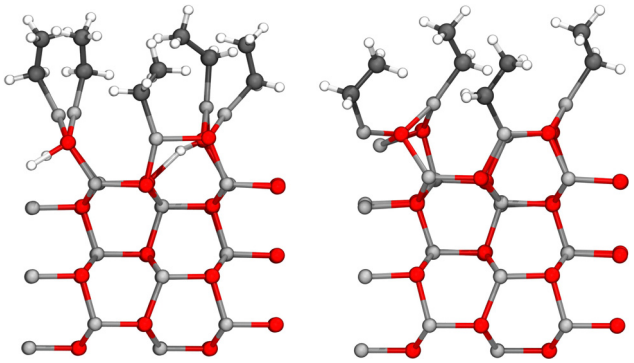

Fig. 8 Structures of ethyl-saturated zinc oxide surface slabs used in this study: case 1 (left) is an estimate of the structure at lower deposition temperatures, whereas case 2 (right) is an estimate of the structure at higher deposition temperatures. The atom colors are the same as those in Fig. 6.

experimental thin films. Hence, ethyl-saturated zinc oxide surface slabs were adopted from the work of Weckman and Laasonen,[35,36] and are presented in Fig. 8. These zinc oxide structures are rigorously validated estimates of thin film structures fabricated at lower (approximately 100–140 °C) and higher (approximately 140–180 °C) deposition temperatures.

The structure deposited at lower temperatures, denoted as case 1, occurs when the hydroxyl groups of the hydroxylated (100) zinc oxide surface react with five diethyl zinc molecules in a ligand-exchange reaction, as shown in eqn (2). Hydroxylation was conducted using four dissociated water molecules on three layers of $(ZnO)_8$. Five ligand-exchange reactions eliminated a total of five hydrogen atoms from the dissociated water from the surface, making the chemical formula of case 1 surface $(ZnO)_{24}(ZnC_2H_5)_5O_4H_3$. Five monoethyl zincs were chosen, as higher concentrations made the structure unstable, thus making the final coverage of monoethyl zinc 7.1 nm^{-2}.[35]

$$||- Zn - OH + Zn(C_2H_5)_2 \rightarrow ||- Zn - O - Zn(C_2H_5) + C_2H_6 \quad (2)$$

In the higher deposition temperature structure, denoted case 2, the structure is similar to case 1, as three layers of $(ZnO)_8$ were initially hydroxylated with four dissociating water molecules. However, at higher deposition temperatures, monoethyl zinc can also react further, thus creating bare zinc atoms on the surface, as illustrated in eqn (3). For the case 2 structure, it was assumed that all hydrogens on the surface were consumed in the ligand-exchange reactions, as presented in eqn (2) and (3). The most stable structure included four monoethyl zinc groups and two zinc atoms; thus, the chemical formula of the surface in case 2 was $(ZnO)_{24}(ZnC_2H_5)_4Zn_2O_4$. The final coverage of monoethyl zinc was 5.7 nm^{-2}.[35]

$$||- Zn - O - Zn(C_2H_5) + ||- Zn - OH \rightarrow (||- Zn - O)_2 - Zn + C_2H_6 \quad (3)$$

3.2.1 Physisorption reactions on both surfaces. Due to the large number of degrees of freedom in the adsorption system, finding an energetically favorable physisorption site is challenging. A combination of molecular dynamics, relaxed surface scans, and constrained geometry optimization was used to identify an exothermic physisorption site for 4-aminophenol. The final configuration for physisorption was always acquired without any constraints, apart from the constraint of holding the lowest layer of atoms in place. For the lower deposition temperature system (denoted case 1), the physisorption energy was −0.2 eV for physisorption with both functional groups. For the higher deposition temperature system (denoted case 2), the physisorption energy was −0.3 eV for both functional groups.

3.2.2 Chemisorption reactions on the case 1 surface. The direct and indirect elimination of the ethyl ligand from the studied surface structures is caused by the donation of a hydrogen atom originally located at either the amino or hydroxyl group of 4-aminophenol. In the direct ligand elimination reaction, 4-aminophenol donates its hydrogen to an ethyl ligand while adsorbing to the surface by utilizing the ligand-exchange reaction, thus removing gaseous ethane from the surface. Indirect ligand elimination begins with the dissociative adsorption of 4-aminophenol, followed by the migration of hydrogen from the hydroxyl group of the surface to the ethyl ligand. This hydroxyl group initially receives its hydrogen atom from the dissociatively adsorbed 4-aminophenol molecule. For indirect ligand elimination in the case 1 structure, there is only one feasible ligand for the hydrogen to migrate from its adsorbing site (*i.e.* the hydroxyl group of the surface), which is the same ligand as in the direct elimination reaction. The reactions and reaction parameters for the direct and indirect elimination reaction pathways are illustrated in Fig. 9 and 10.

3.2.3 Chemisorption reactions on the case 2 surface. Both the direct and indirect elimination of the ethyl ligand are also available on the case 2 surface. After dissociative adsorption of the indirect ligand elimination reaction path, there are three available ligands for hydrogen migration, from which one is the same ligand as in the direct elimination reaction. The other two are neighboring ligands with a feasible pathway for the adsorbed hydrogen to migrate to. All studied reaction pathways for the elimination reaction through hydrogen donation are presented in Fig. 11, where the functional group of 4-aminophenol that donates a hydrogen atom is the hydroxyl group, and in Fig. 12, where the amino group of 4-aminophenol donates a hydrogen atom.

4 Discussion

4.1 Gas-phase model

The gas-phase reactions between diethyl zinc and either hydroquinone or 4-aminophenol proceeded as expected. Either amino or hydroxyl groups donated hydrogen to eliminate ethane from diethyl zinc. Simultaneously, oxygen or nitrogen formed a bond with the zinc of diethyl zinc. All of the studied gas-phase reactions were exothermic. The hydroxyl groups of 4-aminophenol and hydroquinone have similar activation and

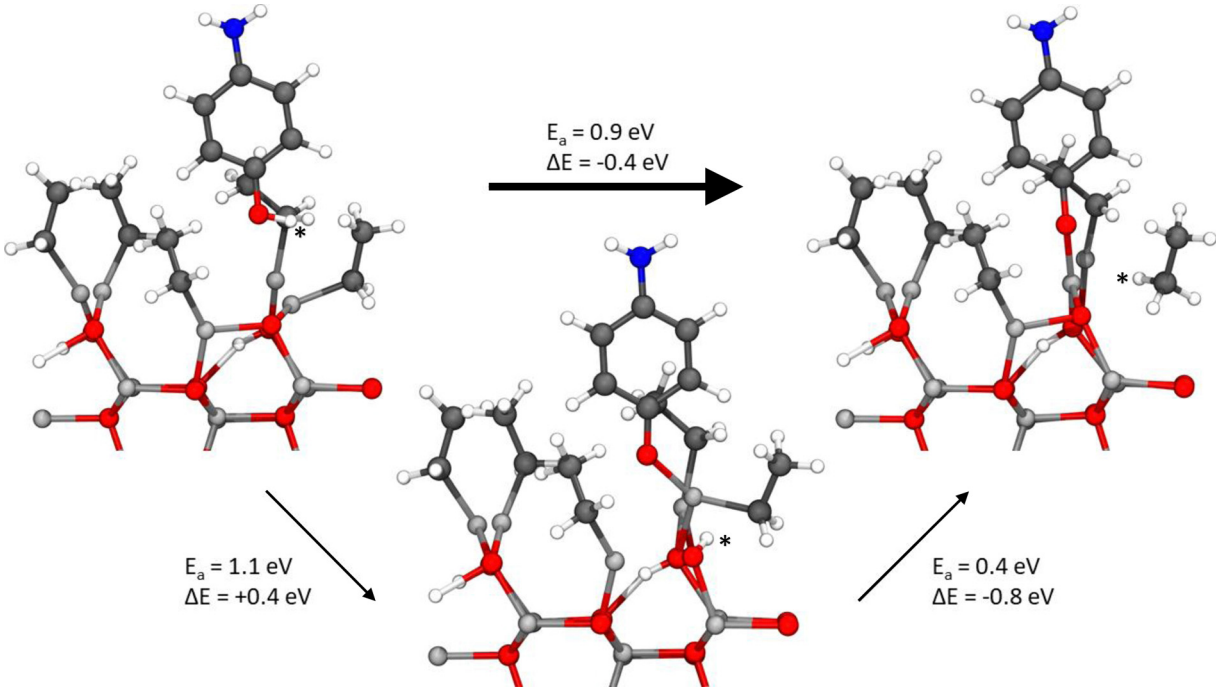

Fig. 9 Reaction pathways for the direct and indirect ligand elimination reactions on the case 1 surface, when the hydroxide group of the 4-aminophenol acts as the hydrogen-donating group. This hydrogen atom can be donated either directly from the physisorbed 4-aminophenol, or it can be initially chemisorbed to an oxygen atom in the surface structure, from where it will migrate to the ethyl ligand. The atom colors are the same as those in Fig. 6. The most feasible reaction pathway is shown in bold. Migrating hydrogen atoms are marked with an asterisk.

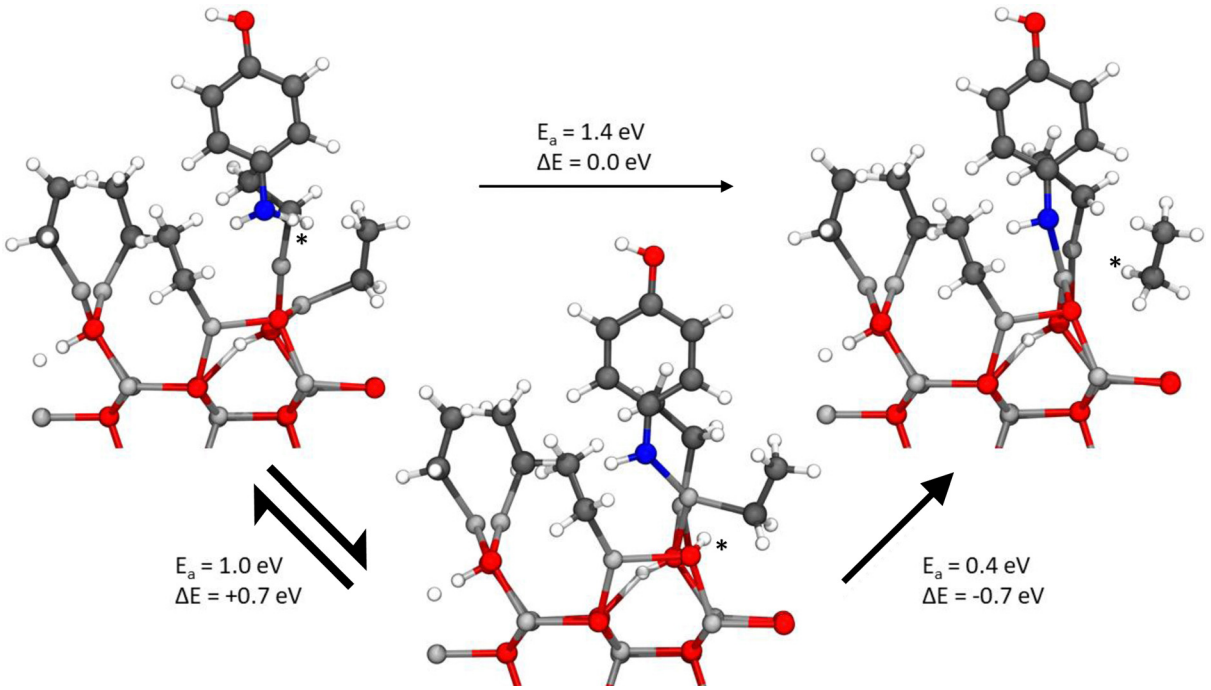

Fig. 10 Reaction pathways for the direct and indirect ligand elimination reactions on the case 1 surface, when the amino group of the 4-aminophenol acts as the hydrogen-donating group. This hydrogen atom can be donated either directly from the physisorbed 4-aminophenol, or it can be initially chemisorbed to an oxygen atom in the surface structure, from where it will migrate to the ethyl ligand. The atom colors are the same as those in Fig. 6. The most feasible reaction pathway is shown in bold. Migrating hydrogen atoms are marked with an asterisk.

reaction energies. Therefore, the surface model was investigated using only 4-aminophenol as the organic precursor.

The amino group of 4-aminophenol reacts more slowly than the hydroxide group, both kinetically and thermodynamically.

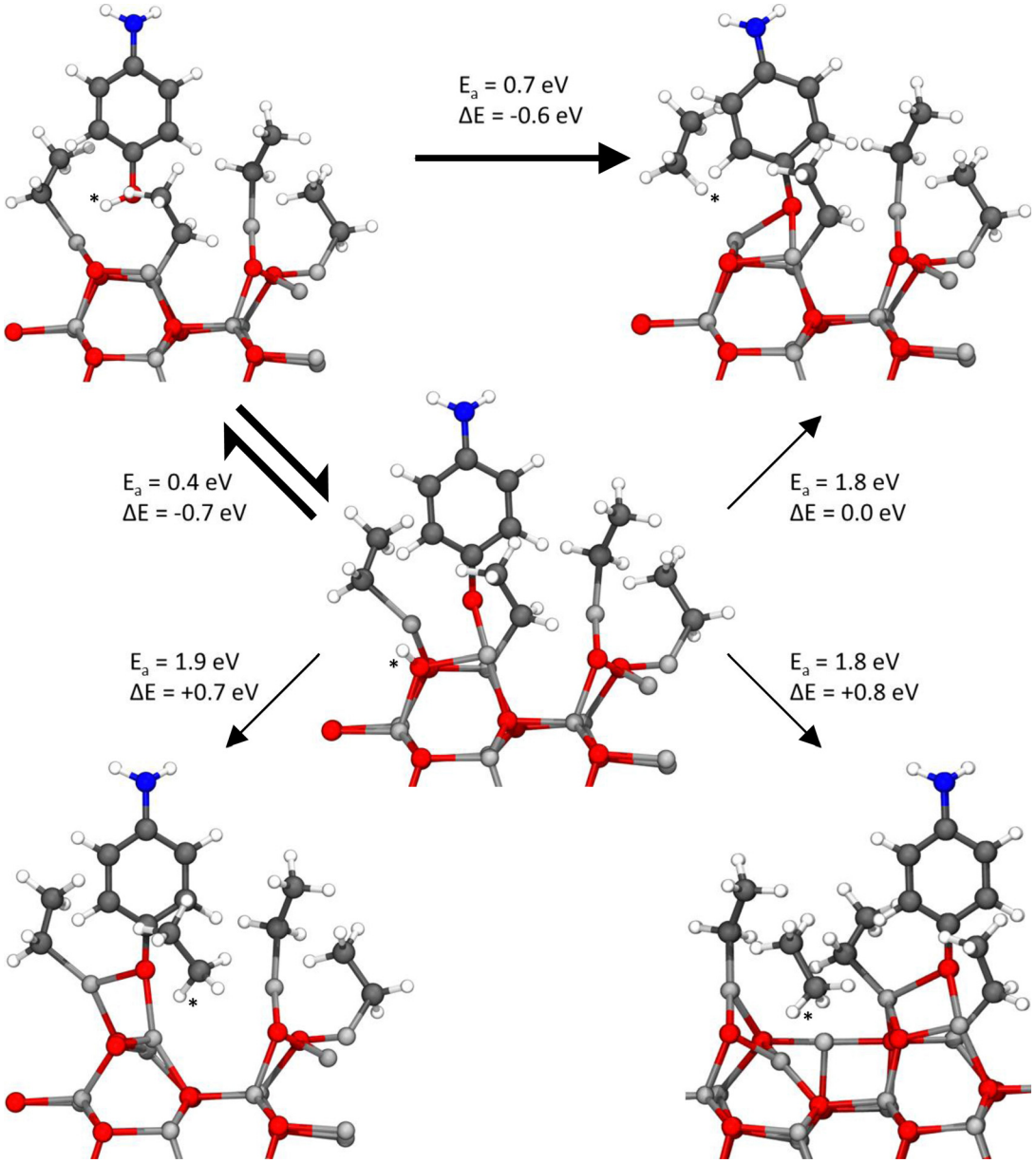

Fig. 11 Reaction pathways for the direct and indirect ligand elimination reactions on the case 2 surface, initiated by the donation of a hydrogen atom from the 4-aminophenol's hydroxide group. The ligand-exchange reaction is hindered by dissociative adsorption, which will lead to a reverse reaction back to the initial state or to a very slow hydrogen migration to the ethyl ligand. The atom colors are the same as those in Fig. 6. The most feasible reaction pathway is shown in bold. Migrating hydrogen atoms are marked with an asterisk.

This result suggests that 4-aminophenol first reacts with its hydroxyl group. According to our surface model, additional surface reaction pathways are available at the interface between zinc oxide and the organic layer of these films, which are not taken into account in the gas-phase model; however, these do not change this result. The relatively high activation energies, especially for the reactions of the amino group, are in agreement with the slow growth of the zincone thin film presented by Sood *et al.*[13] Interestingly, the tendency for 4-aminophenol to react with the hydroxyl rather than the amino group first has been discovered computationally also for titanicone[17] and alucone[18,19] hybrid thin films. Due to the amorphous structure[13] of these films, the growth should be more polymer-like in later precursor pulses, which in practice corresponds to more degrees of freedom for the reactants. This further indicates that gas-phase reactions are beneficial in the discovery of the growth reactions in later pulses, as they offer a hard limit on the effect of degrees of freedom for the system, as an amorphous or crystal structure is always more rigid than a gas-phase structure.

4.2 Surface model

At the higher ethyl-ligand concentration surface (case 1), the most feasible reaction path for 4-aminophenol adsorption

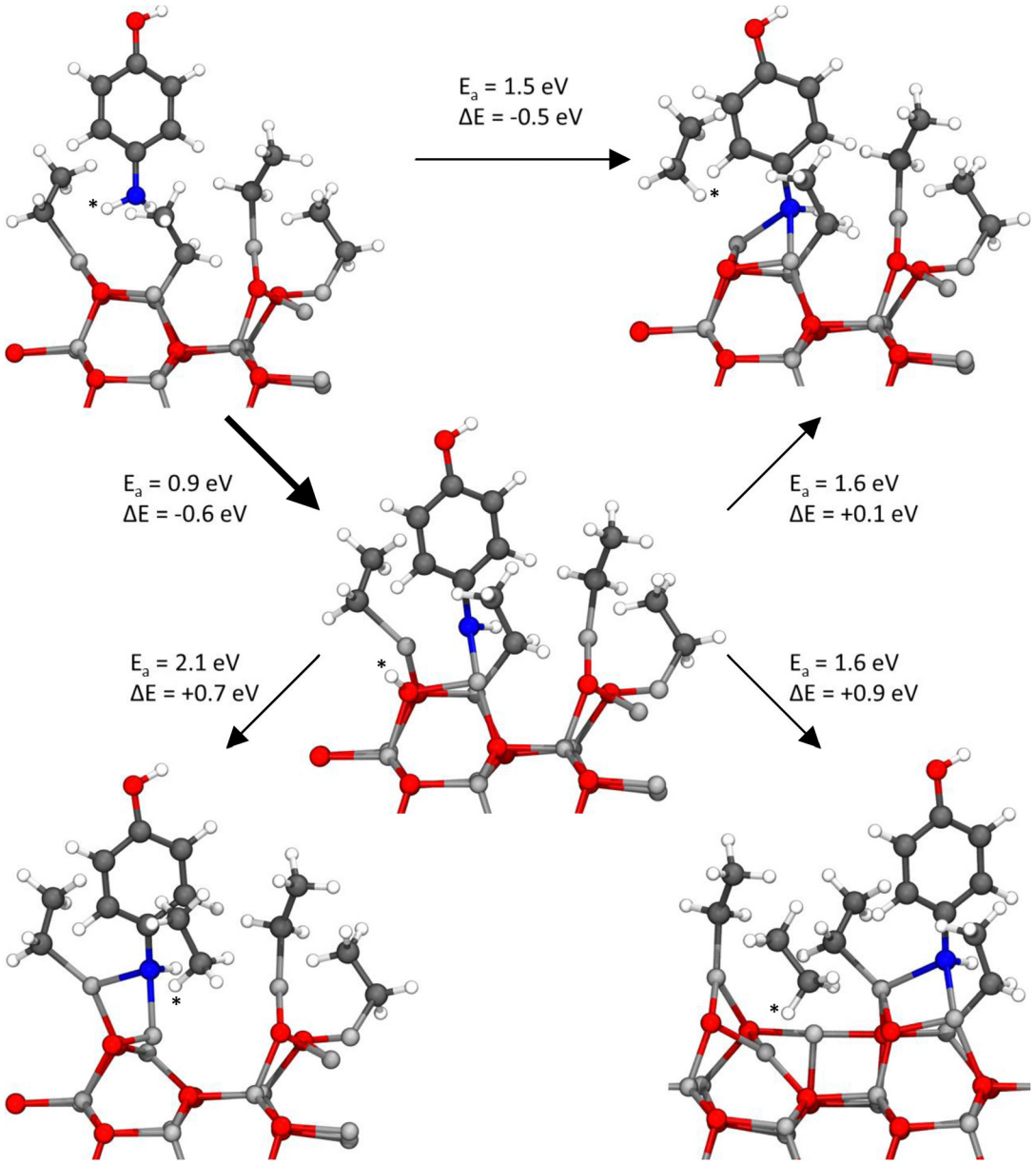

Fig. 12 Reaction pathways for the direct and indirect ligand elimination reactions on the case 2 surface, initiated by donation of a hydrogen atom from the amino group of 4-aminophenol. The activation energies of these reactions are relatively high, and therefore, the reactions of the hydroxyl group presented in Fig. 11 are significantly more feasible on the case 2 surface. The atom colors are the same as in Fig. 6. The most feasible reaction pathway is in bold. The migrating hydrogen atom is marked with an asterisk.

utilizes an exothermic ligand-exchange reaction to react with the hydroxyl group first, with an activation energy of 0.9 eV. For reactions with the hydroxyl group, this reaction path is more feasible than the indirect reaction pathway, which starts with the dissociation reaction, due to the lower activation energy of the reaction. For the amino group on the case 1 surface, the high 1.4 eV activation energy of the direct ligand-exchange reaction causes the dissociation reaction to be the most viable reaction path. However, the viability of this reaction path to eliminate ethane from the surface is hindered by the fact that the desorption of molecular 4-aminophenol (with an activation energy of 0.3 eV) is approximately equal in reaction rate to the migration of hydrogen (with an activation energy of 0.4 eV), which eliminates ethane from the surface. This causes a dynamic reaction, where the reaction alternates between the initial physisorbed state and the dissociatively chemisorbed state, and approximately half of the dissociatively adsorbed 4-aminophenol proceeds to eliminate the ethyl ligand as ethane.

To summarize, on the case 1 surface, the main growth reaction of the hybrid thin film is the ligand-exchange reaction, where 4-aminophenol first reacts with its hydroxyl group. The ALD/MLD process is mainly driven by reaction kinetics due to the relatively short pulsing times, and the 0.9 eV barrier of the direct ligand elimination is the lowest on the case 1 surface.

For the reaction at the lower ethyl-ligand concentration surface (case 2), the situation is more complex. The most feasible reaction path to remove ethane from the surface is the direct ligand elimination reaction of the hydroxyl group of 4-aminophenol. However, this reaction path is hindered by the dissociation reaction, which has a lower reaction barrier of 0.4 eV, but does not proceed to hydrogen migration to eliminate ethane due to a high 1.8 eV reaction barrier. As the relatively small physisorption energy of 4-aminophenol makes physisorption non-spontaneous when entropy is taken into consideration, only a small fraction of ligand elimination reactions occur, while the majority of the reactions occur in equilibrium between the gas phase, physisorbed state, and dissociatively chemisorbed state. This tendency to get trapped in a dissociatively adsorbed state was even more noticeable when the amino group reacted first. For the amino group, dissociative adsorption is the only reaction step with an activation energy below 1.5 eV. Thus, ligand elimination *via* the amino group reacting first is unlikely to occur due to the high activation energies of both reaction paths.

As the first pulse of the ALD/MLD thin film growth is being built on the zinc oxide surface, the first precursor pulse is responsible for surface reactions that may not be present in later precursor pulses. Therefore, these reactions can be crucial for the fabrication of superlattices, where a very thin organic layer alternates with a much thicker inorganic layer. For the investigation of hybrid thin films with higher concentrations of organic layers, both the gas-phase and surface models yield similar results for ligand elimination when the reactions involving the zinc oxide layer, which is not present in further precursor pulses, are excluded from the results. This result suggests that the more computationally feasible gas-phase model can provide relevant results regarding the growth of hybrid thin films.

4.3 Further reactions

In this study, one of the monoethyl zincs is reacting with 4-aminophenol, which corresponds to an ethyl coverage of 1/5 in case 1 and 1/4 in case 2. There is quite a high repulsion present on the surface; therefore, the possibility of more 4-aminophenols reacting with the surface is very low. Karttunen *et al.*[15] studied superlattice structures fabricated from diethyl zinc, water, and hydroquinone. They discovered that when the zinc surface is saturated with hydroxyl groups instead of ethyl ligands, 1/2 of the monoethyl zinc react with the hydroxyl groups of hydroquinone. As the repulsion forces are noticeably higher on ethyl- than on hydroxyl-saturated zinc oxide surface, the coverages presented in this study are in agreement with the results of Karttunen *et al.*

In contrast to superlattice structures, in the studied hybrid thin film surface structures, the unreacted ethyl ligands cannot escape from the surface, as there is no future water precursor for ALD pulses, which could remove ethyl ligands as gaseous ethane. Thus, all of the reactions of ethyl ligands occur with an organic precursor, which is either 4-aminophenol or hydroquinone. In addition, a small physisorption energy of −0.2 or −0.3 eV is not sufficient to account for the entropy of these relatively large organic molecules, making the physisorption non-spontaneous. As the reaction of the first molecule in the unit cell is energetically demanding, the possibility of the second 4-aminophenol adsorbed within the same unit cell seems highly unlikely from an energetic point of view because the repulsion on the surface increases significantly after the adsorption of the first 4-aminophenol, thus hindering the adsorption of the second 4-aminophenol. This makes the growth direction vertical, even though there are still seemingly available reaction sites on the surface. For comparison, these reaction sites are also available in ALD thin films, where the organic precursor is replaced with water,[37] which is much smaller in size. This also indicates that repulsion plays a significant role in the final structure of hybrid thin films. To summarize, the next reaction should be the diethyl zinc precursor that reacts with the 4-aminophenol adsorbed on the surface. As the 4-aminophenol is more likely to react first with the hydroxyl group, diethyl zinc should react with the amino group.

5 Conclusions

In this study, we extensively investigated the growth reactions of hybrid thin films fabricated with diethyl zinc and either hydroquinone or 4-aminophenol. We employed both gas-phase and surface models. According to the gas-phase models, diethyl zinc reacts similarly with the hydroxyl groups of both hydroquinone and 4-aminophenol. In both gas-phase and surface models, zinc ethyl reacts more rapidly with the hydroxyl group than with the amino group of 4-aminophenol, which suggests that the adsorbed 4-aminophenol in the thin film should align with the hydroxyl group positioned down and the amino group positioned up. In addition, the rate of the total hybrid thin film growth reaction was hindered by the low reaction speed between diethyl zinc and the amino group of 4-aminophenol, which was observed in both gas-phase and surface models.

The oxygen in the zinc oxide layer can accept a hydrogen atom from the dissociating 4-aminophenol, thus hindering the elimination of the ethyl ligand as gaseous ethane, as the reaction can become trapped between the physisorbed and dissociatively adsorbed states. This effect, in conjunction with the relatively high reaction barriers and non-spontaneous physisorption, results in the overall slow growth of the hybrid thin film. For superlattice structures, where zinc oxide layers are separated by only a single organic layer, this effect is present in every deposition of the organic precursor. However, this effect should be absent from the later precursor pulses of hybrid thin films, as the oxygen of the zinc oxide should be available only for the initial organic precursor pulse, as the precursors used do not contain water apart from the initial ALD layer of zinc oxide.

The surface model provides detailed information about the growth reactions at the interface between the zinc oxide and 4-aminophenol layers. This information is important, especially in the study of superlattice structures, and much of this information is not present in the gas-phase models. However,

due to the absence of oxygen in later precursor pulses and the higher number of degrees of freedom precursors have when bonding in an amorphous form in comparison to a more rigid crystalline structure, a gas-phase model should be sufficient for investigating the polymer-like growth of the hybrid thin film. Hence, this study investigated hybrid thin films using both approaches to gain comprehensive knowledge of the complex phenomena that occur during the hybrid thin film deposition process.

Author contributions

Mario Mäkinen: conceptualization, methodology, software, validation, formal analysis, investigation, data curation, writing – original draft, writing – review & editing, visualization, and funding acquisition. Timo Weckman: conceptualization, methodology, software, and supervision. Kari Laasonen: conceptualization, resources, writing – review & editing, supervision, project administration, and funding acquisition.

Conflicts of interest

There are no conflicts to declare.

Acknowledgements

This work was supported by the Finnish Cultural Foundation. The authors wish to acknowledge the CSC - IT Center for Science, Finland, for the computational resources. Timo Weckman acknowledges Jane and Aatos Erkko Foundation for the funding for the LACOR project.

References

1 M. Mäkinen, Structural Data for the Zincone ALD/MLD Hybrid Thin Film Growth Reactions, 2023, *Harvard Dataverse, V2*, DOI: **10.7910/dvn/wfvehm**.
2 R. L. Puurunen, *J. Appl. Phys.*, 2005, **97**, 121301.
3 P. Sundberg and M. Karppinen, *Beilstein J. Nanotechnol.*, 2014, **5**, 1104–1136.
4 J. Multia and M. Karppinen, *Adv. Mater. Interfaces*, 2022, **9**, 2200210.
5 T. Tynell and M. Karppinen, *Semicond. Sci. Technol.*, 2014, **29**, 043001.
6 A. J. Karttunen, T. Tynell and M. Karppinen, *Nano Energy*, 2016, **22**, 338–348.
7 F. Krahl, A. Giri, J. A. Tomko, T. Tynell, P. E. Hopkins and M. Karppinen, *Adv. Mater. Interfaces*, 2018, **5**, 1701692.
8 B. Yoon, Y. Lee, A. Derk, C. Musgrave and S. George, *ECS Trans.*, 2011, **33**, 191–195.
9 B. Yoon, B. H. Lee and S. M. George, *ECS Trans.*, 2011, **41**, 271.
10 J. Liu, B. Yoon, E. Kuhlmann, M. Tian, J. Zhu, S. M. George, Y.-C. Lee and R. Yang, *Nano Lett.*, 2013, **13**, 5594–5599.
11 T. Tynell, A. Giri, J. Gaskins, P. E. Hopkins, P. Mele, K. Miyazaki and M. Karppinen, *J. Mater. Chem. A*, 2014, **2**, 12150–12152.
12 A. J. Karttunen, L. Sarnes, R. Townsend, J. Mikkonen and M. Karppinen, *Adv. Electron. Mater.*, 2017, **3**, 1600459.
13 A. Sood, P. Sundberg and M. Karppinen, *Dalton Trans.*, 2013, **42**, 3869–3875.
14 P. Sundberg, A. Sood, X. Liu and M. Karppinen, *Dalton Trans.*, 2013, **42**, 15043–15052.
15 A. J. Karttunen, T. Tynell and M. Karppinen, *J. Phys. Chem. C*, 2015, **119**, 13105–13114.
16 D. Choudhury, G. Rajaraman and S. K. Sarkar, *RSC Adv.*, 2015, **5**, 29947–29952.
17 A. Tanskanen, P. Sundberg, M. Nolan and M. Karppinen, *Thin Solid Films*, 2021, **736**, 138896.
18 A. Muriqi, M. Karppinen and M. Nolan, *Dalton Trans.*, 2021, **50**, 17583–17593.
19 F. Yang, J. Brede, H. Ablat, M. Abadia, L. Zhang, C. Rogero, S. D. Elliott and M. Knez, *Adv. Mater. Interfaces*, 2017, **4**, 1700237.
20 J. Enkovaara, C. Rostgaard, J. J. Mortensen, J. Chen, M. Dułak, L. Ferrighi, J. Gavnholt, C. Glinsvad, V. Haikola, H. A. Hansen, H. H. Kristoffersen, M. Kuisma, A. H. Larsen, L. Lehtovaara, M. Ljungberg, O. Lopez-Acevedo, P. G. Moses, J. Ojanen, T. Olsen, V. Petzold, N. A. Romero, J. Stausholm-Møller, M. Strange, G. A. Tritsaris, M. Vanin, M. Walter, B. Hammer, H. Häkkinen, G. K. H. Madsen, R. M. Nieminen, J. K. Nørskov, M. Puska, T. T. Rantala, J. Schiøtz, K. S. Thygesen and K. W. Jacobsen, *J. Phys.: Condens. Matter*, 2010, **22**, 253202.
21 A. H. Larsen, J. J. Mortensen, J. Blomqvist, I. E. Castelli, R. Christensen, M. Dułak, J. Friis, M. N. Groves, B. Hammer, C. Hargus, E. D. Hermes, P. C. Jennings, P. B. Jensen, J. Kermode, J. R. Kitchin, E. L. Kolsbjerg, J. Kubal, K. Kaasbjerg, S. Lysgaard, J. B. Maronsson, T. Maxson, T. Olsen, L. Pastewka, A. Peterson, C. Rostgaard, J. Schiøtz, O. Schütt, M. Strange, K. S. Thygesen, T. Vegge, L. Vilhelmsen, M. Walter, Z. Zeng and K. W. Jacobsen, *J. Phys.: Condens. Matter*, 2017, **29**, 273002.
22 W. Humphrey, A. Dalke and K. Schulten, *J. Mol. Graphics*, 1996, **14**, 33–38.
23 J. P. Perdew, K. Burke and M. Ernzerhof, *Phys. Rev. Lett.*, 1996, **77**, 3865–3868.
24 A. Calzolari, A. Ruini and A. Catellani, *J. Am. Chem. Soc.*, 2011, **133**, 5893–5899.
25 S. L. Dudarev, G. A. Botton, S. Y. Savrasov, C. J. Humphreys and A. P. Sutton, *Phys. Rev. B: Condens. Matter Mater. Phys.*, 1998, **57**, 1505–1509.
26 A. Tkatchenko and M. Scheffler, *Phys. Rev. Lett.*, 2009, **102**, 073005.
27 G. Henkelman, B. P. Uberuaga and H. Jónsson, *J. Chem. Phys.*, 2000, **113**, 9901–9904.
28 E. Bitzek, P. Koskinen, F. Gähler, M. Moseler and P. Gumbsch, *Phys. Rev. Lett.*, 2006, **97**, 170201.
29 W. Tang, E. Sanville and G. Henkelman, *J. Phys.: Condens. Matter*, 2009, **21**, 084204.
30 A. J. Cohen, P. Mori-Sánchez and W. Yang, *Science*, 2008, **321**, 792–794.

31 D. G. Sangiovanni, R. Faccio, G. K. Gueorguiev and A. Kakanakova-Georgieva, *Phys. Chem. Chem. Phys.*, 2023, **25**, 829–837.
32 R. J. Maurer, C. Freysoldt, A. M. Reilly, J. G. Brandenburg, O. T. Hofmann, T. Björkman, S. Lebègue and A. Tkatchenko, *Annu. Rev. Mater. Res.*, 2019, **49**, 1–30.
33 J. A. Garrido Torres, P. C. Jennings, M. H. Hansen, J. R. Boes and T. Bligaard, *Phys. Rev. Lett.*, 2019, **122**, 156001.
34 R. Kronberg and K. Laasonen, *ACS Catal.*, 2021, **11**, 8062–8078.
35 T. Weckman and K. Laasonen, *J. Phys. Chem. C*, 2016, **120**, 21460–21471.
36 T. Weckman and K. Laasonen, *J. Phys. Chem. C*, 2018, **122**, 7685–7694.
37 A. J. M. Mackus, C. MacIsaac, W.-H. Kim and S. F. Bent, *J. Chem. Phys.*, 2016, **146**, 052802.